Travel-time sensitivity kernels versus diffraction patterns obtained through double beam-forming in shallow water

Ion Iturbe[a)]
GIPSA Laboratory, INPG–CNRS, 961 rue de la Houille Blanche, Domaine Universitaire, BP 46, 38402 Saint Martin d'Heres, France

Philippe Roux and Jean Virieux
LGIT, Universite Joseph Fourier–CNRS, 1381 rue de la Piscine, Saint Martin d'Heres, 38400 France

Barbara Nicolas
GIPSA Laboratory, INPG–CNRS, 961 rue de la Houille Blanche, Domaine Universitaire, BP 46, 38402 Saint Martin d'Heres, France

(Received 5 August 2008; revised 22 May 2009; accepted 27 May 2009)

In recent years, the use of sensitivity kernels for tomographic purposes has been frequently discussed in the literature. Sensitivity kernels of different observables (e.g., amplitude, travel-time, and polarization for seismic waves) have been proposed, and relationships between adjoint formulation, time-reversal theory, and sensitivity kernels have been developed. In the present study, travel-time sensitivity kernels (TSKs) are derived for two source-receiver arrays in an acoustic waveguide. More precisely, the TSKs are combined with a double time-delay beam-forming algorithm performed on two source-receiver arrays to isolate and identify each eigenray of the multipath propagation between a source-receiver pair in the acoustic waveguide. A relationship is then obtained between TSKs and diffraction theory. It appears that the spatial shapes of TSKs are equivalent to the gradients of the combined direction patterns of the source and receiver arrays. In the finite-frequency regimes, the combination of TSKs and double beam-forming both simplifies the calculation of TSK and increases the domain of validity for ray theory in shallow-water ocean acoustic tomography. © *2009 Acoustical Society of America.* [DOI: 10.1121/1.3158922]

PACS number(s): 43.60.Fg, 43.60.Rw [WLS] Pages: 713–720

I. INTRODUCTION

The resolution limit of travel-time tomography has been studied from various aspects.[1–3] This investigation essentially relies on the specific, maybe paradoxical, nature of travel-times, as extracted from time-series recordings. Once picked, travel-times lose the frequency information of the time series. For example, in seismology, choosing times from high-frequency impulsive seismograms or from broad-band low-frequency seismograms will certainly have an impact on the tomographic resolution. However, the frequency information is not used in the travel-time tomography machinery based on ray theory (for example, see Ref. 4). *Ad hoc* procedures for introducing frequency information have been designed[5] with the so-called fat-ray concept, based on reconstruction assumptions. The more physical concept of the wave path, as related to the wave propagation properties, was introduced by Woodward,[6] which is closely related to Fresnel tomography in optics.[7] In recent years, this finite-frequency influence has been systematically investigated for the different observables (i.e., time, polarization, amplitude, and anisotropy) in different studies, suggesting that higher resolution images can be obtained from this improved description of wave propagation physics (see Ref. 8 for a general review).

Based on single-scattering effects, sensitivity kernels have been introduced and different computational techniques have been devised from ray theory as paraxial theory[9] or exact ray theory[10] to numerical tools.[11] Different studies[12] have questioned the differential techniques used for the construction of these sensitivity kernels, with the emphasis on the so-called banana-doughnut paradox: for travel-times, the sensitivity kernel is zero on the ray connecting the source and the receiver. Other studies[13] have shown that the travel-time tomographic problem with the specific density of stations and sources encountered in seismology prevents an improvement of resolution. Overcoming these limitations of data quality requires a denser deployment of sources and receivers, which can be expensive.

Similar to seismic studies, consideration of arrays of sources and receivers is a classical approach in underwater acoustics.[14] Wave-propagation problems can lead to similar features as in geophysics, and we would like to investigate the effects of the finite size of the source and/or receiver arrays in underwater tomographic reconstructions. The concept of sensitivity kernels has been applied recently to this field,[15] and quite exciting theoretical and experimental investigations have led to fruitful achievements with links to time-reversal theory,[16,17] adjoint methods,[11] and acoustic and seismic imagings[18] or medical imaging.[19–21]

In the present study, the relationships between travel-time sensitivity kernel (TSK) reconstruction and diffraction theory in the context of shallow underwater acoustics is de-

[a)]Author to whom correspondence should be addressed. Electronic mail: ion.iturbe@gipsa-lab.inpg.fr

fined when the transfer function of the waveguide is recorded between source and receiver arrays. We show that the spatial shapes of TSKs are equivalent to the gradient of the combined diffraction pattern of the arrays. This relationship is exact when working with a point-to-point approach (using only one source and one receiver), and it becomes more complex and approximate when TSKs are calculated between two source and receiver arrays.

In a shallow-water environment, array processing using source and/or receiver arrays is necessary to improve the separation of the different ray paths. One standard array processing method is time-delay beam-forming on the receiver array, to separate the ray paths according to their receiver angles.[22] Recently, Roux *et al.*[23] proposed a more sophisticated time-delay double beam-forming (DBF) algorithm, based on spatial reciprocity, which takes advantage of both receiver and source arrays. The DBF algorithm can be applied when the entire transfer matrix is measured between each pair of source-receiver transducers. DBF consists of transforming the three-dimensional (3D) data space from source depth, receiver depth, and time into a new 3D space that is related to ray propagation, described by the beam-formed variables: source angle, receiver angle and time. As a consequence, every eigenray of the multipath propagation for a source-receiver pair is identified and isolated through DBF according to the receiver and source angles.

In their very recent study, Roux *et al.*[23] went one step further. Every eigenray isolated through DBF processing became free from any interference effects due to multipath propagation. Furthermore, DBF processing provides array gain and robustness, since every DBF eigenray arises from the summation of a large number of time-delayed source-to-receiver signals. Thus, both the amplitude and phase of the DBF eigenray can be followed as a function of dynamic ocean fluctuations, when, for example, internal waves locally perturb the sound-speed profile (see Fig. 7 of Ref. 23).

The stability and robustness of DBF processing can lead to important consequences for future studies relating to ocean acoustic tomography. To date, travel-time tomography has mainly been performed from echo arrival peaking through point-to-point measurements. Indeed, only the envelope of the demodulated signal was a robust observable, regarding signal-to-noise ratio issues and rapidly changing ocean fluctuations (e.g., gravity waves at the ocean surface). The use of source-receiver arrays now allows the travel-time fluctuations to be measured as phase changes in the DBF signal, providing travel-time measurements with greater accuracy. Indeed, travel-time change measured through the phase has an accuracy driven by the carrier frequency F_c of the signal, while travel-time changes measured through the envelope of the demodulated signal depend on the frequency bandwidth $\delta f < F_c$.

Note, however, that the travel-time change measured through the phase of an eigenray is not a measurement of phase velocity, as classically defined as the phase speed along the waveguide axis. For rays, the phase velocity along the waveguide axis is $c(z_0)/\cos(\theta_0)$, where $c(z_0)$ is the depth-dependent sound-speed profile at the source/receiver depth z_0, and θ_0 is the launch/receiver eigenray angle. In water, the bulk modulus shows nearly no frequency dependence, which means that wave dispersion in the ocean comes only from reverberation on interfaces and/or refraction due to sound-speed gradients. As a consequence, and with water being nondispersive, the group and phase velocities are the same along the ray path of an eigenray. The measurement of travel-time that changes through the phase of the DBF eigenray is then just a more accurate observable for the measuring of changes in the group velocity.

In the context of DBF, the sensitivity kernel is no longer point-to-point but relies on all source-receiver time series. The kernels are computed based on the concept that the processed signal is a linear combination of the time-delayed signals between all sources and receivers. Throughout this study, we concentrate on the physics that connects TSKs and Fresnel diffraction in the context of source-receiver arrays and a multipath environment in which DBF is performed to identify and isolate every eigenray. We show that TSKs associated with DBF result in increased spatial diversity of the sensitivity kernels which improves the range of validity of the ray theory for shallow-water acoustic tomography in the low-frequency regime.

This report is divided into four sections. Following this introduction (Sec. I), in Sec. II, the relationship between the TSK and the acoustic diffraction pattern is obtained for the point-to-point case. In Sec. III, the discussion is extended to source-receiver arrays through the DBF algorithm, which provides identification of every eigenray in the waveguide. The discussion continues in Sec. IV relating to the use of DBF in the context of shallow-water ocean acoustic tomography.

II. TSKs VERSUS DIFFRACTION

In this section, we investigate the links between TSKs and acoustic diffraction patterns for point-to-point, source-receiver configurations. Starting from the review of Skarsoulis *et al.*,[15] who first introduced TSKs into ocean acoustic tomography, we show here that in the far-field approximation, the TSK is the gradient of the diffraction pattern, corrected by a spatial factor.

The TSK is a measure of the travel-time perturbation of an acoustic path versus any spatial perturbation of the range-dependent and depth-dependent sound-speed profile. The pressure-field in the waveguide is expressed as the convolution of the source distribution over the source volume and the Green's function $G(\mathbf{r},\mathbf{r}_s,\omega)$. Under the first Born approximation, the Green's function perturbation δG has a linear relationship with the perturbation of the sound-speed distribution, δc, according to

$$\delta G(\mathbf{r}_r,\mathbf{r}_s,\omega) = -2\omega^2 \int\int\int G(\mathbf{r},\mathbf{r}_s,\omega) G(\mathbf{r}_r,\mathbf{r},\omega) \frac{\delta c(\mathbf{r})}{c^3(\mathbf{r})} dV(\mathbf{r}). \tag{1}$$

The temporal expression of the pressure-field $p(t)$ is written as the inverse Fourier transform of the frequency-domain pressure-field through

$$p(t) = \frac{1}{2\pi}\int G(\mathbf{r}_r,\mathbf{r}_s,\omega)P_s(\omega)e^{j\omega t}d\omega, \tag{2}$$

where $P_s(\omega)$ is the source spectrum. Then, a variation in the pressure-field δp has a linear relation with the Green's function perturbation:

$$\delta p(t) = \frac{1}{2\pi}\int \delta G(\mathbf{r}_r,\mathbf{r}_s,\omega)P_s(\omega)e^{j\omega t}d\omega. \tag{3}$$

Equations (3) and (1) provide linear relationship between the pressure-field perturbation and the sound-speed perturbation.

For estimation of the TSK, the perturbation of the travel-time related to the perturbation of the pressure-field needs to be considered. For acoustic propagation, Skarsoulis *et al.*[15] proposed that the travel-time is defined as the peak of the envelope of the demodulated or analytical signal. In the case of strong signal-to-noise ratios, as discussed above, the travel-time change is performed directly as the phase change of the pressure-field. In theory, this phase change can be measured at any time of the pressure-field. We chose to measure the travel-time change at the cycle peak of maximal amplitude τ_i. In this case, the relationship between the travel-time perturbation and the signal perturbation simplifies to

$$\delta\tau_i = -\frac{\delta\dot{p}_i}{\ddot{p}_i}, \tag{4}$$

where $\ddot{p}_i$ is the second-order derivative of the pressure-field p at time τ_i, and $\delta\dot{p}_i$ is the first-order derivative of the pressure-field perturbation δp evaluated at time τ_i [Eq. (3)]. Note that as compared to Skarsoulis *et al.*,[15] where they dealt with analytic complex signals, here the p and δp defined in Eqs. (2) and (3) are real quantities.

Combining Eqs. (1)–(4), the travel-time perturbation $\delta\tau_i$ is related to a perturbation of a sound-speed distribution δc through the integral:

$$\delta\tau_i = \int\int\int \delta c(\mathbf{r})K_i(\mathbf{r},\mathbf{r}_s,\mathbf{r}_r)dV(\mathbf{r}), \tag{5}$$

where the expression K_i is the TSK. In Ref. 15, a general formulation of K_i is given for the case of analytic signals. Again, as we only deal with real signals, the TSK K_i simplifies to

$$K_i(\mathbf{r},\mathbf{r}_s,\mathbf{r}_r) = \frac{1}{2\pi}\int \frac{j\omega}{\ddot{p}_i}Q(\mathbf{r},\mathbf{r}_s,\mathbf{r}_r,\omega)e^{j\omega\tau_i}d\omega, \tag{6}$$

where Q is given according to[15]

$$Q(\mathbf{r},\mathbf{r}_s,\mathbf{r}_r,\omega) = G(\mathbf{r},\mathbf{r}_s,\omega)G(\mathbf{r}_r,\mathbf{r},\omega)\frac{2\omega^2 Ps(\omega)}{c^3(\mathbf{r})}. \tag{7}$$

In Fig. 1, the TSK results are illustrated for two different geometries. The first was obtained through numerical simulation. For a given ray path in the waveguide, the TSK is built by computing Green's functions using a parabolic equation code[24] [Fig. 1(a)]. The second geometry was obtained through analytical Green's functions in a free-space medium where the receiver is the image of the actual receiver in the waveguide with respect to the waveguide boundary conditions [pressure release at the air-water interface and rigid bottom, Fig. 1(b)]. Consequently, the travel path in the free-space medium is the unfolded version of the actual travel path in the waveguide. The source signal has a 2.5 kHz central frequency and 4 kHz bandwidth. Interestingly, even if the acoustic fields are different in the two configurations, the two methods give similar TSK patterns away from the waveguide boundaries, where different echoes interfere [Fig. 1(c)].

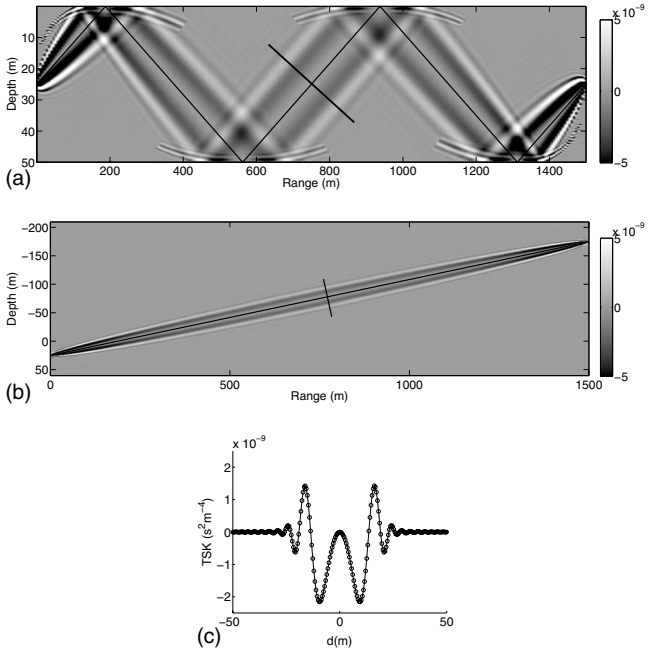

FIG. 1. (a) TSK (s^2 m^{-4}) in a waveguide for a ray path selected between two source-receiver arrays. (b) TSK for the equivalent ray path in free space [note scale change on vertical axis with respect to (a)]. (c) Cross-section of the TSK perpendicular to the ray path along the lines in (a) and (b) at the middle of the source-receiver range. Solid-line corresponds to (a), and circles correspond to (b).

The Green's function we consider in this waveguide is the sum of different eigenray contributions that can be separated through the DBF analysis. Each ray can have a complex trajectory (curved and/or broken lines), which can include rebounds on the waveguide boundaries. As we have been able to separate each ray from other neighboring rays, we can compute the travel-time and amplitude considering reflections at boundaries and/or any variations in speed. For simplicity, we will only consider here a uniform sound-speed and straight rays in the waveguide, although our study can also be extended to refracted rays. As stated above, the group and phase velocities along each eigenray are identical in this shallow-water regime, which means that the free-space approach will provide similar results away from the waveguide interfaces. Therefore, we proceeded with the free-space TSK for our analysis, and we can illustrate the results with the waveguide TSKs in some specific cases. Obviously, the computational costs in a free-space medium, where a simple analytic expression for the pressure-field is available, are much lower than in a waveguide where geometric dispersion has to be taken into account through modes or rays.

The standard well-known shape of the TSK is seen in Fig. 1, for the case of a uniform sound speed c. We observe zero-sensitivity on the ray path that refers to the so-called

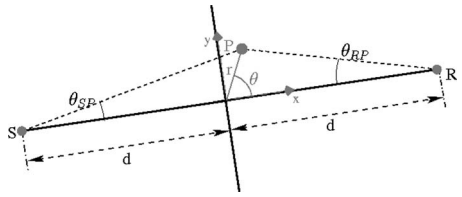

FIG. 2. Schematic of the source (s) and receiver (r) configuration in free space with polar coordinates (r,θ) and the definition of the angles θ_{RP} and θ_{SP}.

banana-doughnut shape of the TSK. A negative sensitivity zone is then seen, which is known as the first Fresnel zone. Higher-order Fresnel zones follow when moving away from the ray path.

On the other hand, the diffraction pattern between the source and the receiver has a maximum on the ray path. Its spatial derivative along a direction perpendicular to the ray is therefore zero on the ray. One may wish to investigate the link between this derivative and the TSK. Following the Huygens–Fresnel principle and invoking reciprocity, the acoustic diffraction pattern between a source and a receiver observed from any point of the medium $\mathbf{r}$ is computed as a product of both the Green's functions at the receiver $\mathbf{r}_r$ and the source $\mathbf{r}_s$:

$$D(\mathbf{r},\mathbf{r}_s,\mathbf{r}_r,\omega)=G(\mathbf{r},\mathbf{r}_s,\omega)G(\mathbf{r},\mathbf{r}_r,\omega). \tag{8}$$

Considering the Green's function in a homogeneous free-space medium:

$$G(\mathbf{r},\mathbf{r}_0,\omega)=\frac{1}{4\pi d(\mathbf{r},\mathbf{r}_0)}e^{-j\omega d(\mathbf{r},\mathbf{r}_0)/c}, \tag{9}$$

it follows that

$$D(\mathbf{r},\mathbf{r}_s,\mathbf{r}_r,\omega)=R(\mathbf{r},\mathbf{r}_s,\mathbf{r}_r)e^{-j\omega\tau(\mathbf{r},\mathbf{r}_s,\mathbf{r}_r)},$$

with

$$R(\mathbf{r},\mathbf{r}_s,\mathbf{r}_r)=\frac{1}{(4\pi)^2 d(\mathbf{r},\mathbf{r}_s)d(\mathbf{r},\mathbf{r}_r)},$$

and

$$\tau(\mathbf{r},\mathbf{r}_s,\mathbf{r}_r)=\frac{d(\mathbf{r},\mathbf{r}_s)+d(\mathbf{r},\mathbf{r}_r)}{c}. \tag{10}$$

Any change in $\mathbf{r}$ along the ray does not produce any phase change in the diffraction pattern D (since τ remains constant), and only produces small and smooth amplitude variations in the far field. On the contrary, a change in $\mathbf{r}$ along a perpendicular direction to the ray path will affect the phase, as investigated by Romanowicz and Snieder[25] and Snieder and Romanowicz[26] when considering seismic velocity perturbations. The gradient of the diffraction D on the perpendicular direction to the ray path is given by

$$\nabla_y D=\nabla D\cdot\boldsymbol{u}_y=[\nabla R-j\omega R\nabla\tau]e^{-j\omega\tau}\cdot\boldsymbol{u}_y, \tag{11}$$

where the $\boldsymbol{u}_y$ vector is the unitary vector along the y-direction shown in Fig. 2. At large distance from the source and receiver, ∇R can be ignored ($\nabla R\ll\omega R\nabla\tau$) and Eq. (11) reduces to

$$\nabla_y D=-j\omega R e^{-j\omega\tau}\nabla\tau\cdot\boldsymbol{u}_y. \tag{12}$$

Inside Eq. (12), there are (1) the propagation terms R and τ, which are related to both of the source/diffractor and receiver/diffractor propagations that determine the phase and amplitude of D; (2) the oblique gradient as the $\nabla\tau\cdot\boldsymbol{u}_y$ term, related to the local perturbations we are interested in. Considering the free-space Green's function G, we can rewrite Eq. (12) as

$$\nabla_y D=-j\omega G(\mathbf{r},\mathbf{r}_s,\omega)G(\mathbf{r},\mathbf{r}_r,\omega)(\nabla\tau\cdot\boldsymbol{u}_y), \tag{13}$$

Comparing Eqs. (7) and (13), we can see that the source-receiver diffraction pattern is proportional to the temporal derivative of Q multiplied by a spatial factor, $\nabla_y\tau$, which is analyzed below. Taking the reference point on the center of the ray-path trajectory, τ is written in polar coordinates (r,θ) as (see Fig. 2)

$$\tau(\mathbf{r},\mathbf{r}_s,\mathbf{r}_r)=\frac{\sqrt{r^2+d^2-2rd\cos(\pi-\theta)}+\sqrt{r^2+d^2-2rd\cos(\theta)}}{c}. \tag{14}$$

Taking into account that $\cos(\pi-\theta)=-\cos(\theta)$ and $\sin(\pi-\theta)=\sin(\theta)$, the gradient of τ in polar coordinates becomes

$$\nabla\tau(\mathbf{r},\mathbf{r}_s,\mathbf{r}_r)=\begin{pmatrix}\dfrac{r+d\cos\theta}{c\sqrt{r^2+d^2+2rd\cos(\theta)}}+\dfrac{r-d\cos\theta}{c\sqrt{r^2+d^2-2rd\cos(\theta)}}\\ \dfrac{-d\sin\theta}{c\sqrt{r^2+d^2+2rd\cos(\theta)}}+\dfrac{d\sin\theta}{c\sqrt{r^2+d^2-2rd\cos(\theta)}}\end{pmatrix}. \tag{15}$$

Calculating the directional gradient in the y-direction, we obtain

$$\nabla_y\tau=\nabla\tau\cdot\vec{u_y}=\frac{r\sin\theta}{c\sqrt{r^2+d^2+2rd\cos(\theta)}}+\frac{r\sin\theta}{c\sqrt{r^2+d^2-2rd\cos(\theta)}}=\frac{\sin\theta_{SP}+\sin\theta_{RP}}{c}, \tag{16}$$

where θ_{SP} and θ_{RP} are the source and receiver angles shown in Fig. 2. Finally, substituting Eq. (16) into Eq. (13) for the directional gradient of the diffraction pattern, and computing the inverse Fourier transform, we obtain the complete expression of the gradient of the diffraction pattern in the time domain as

$$\nabla_y D(\mathbf{r},\mathbf{r}_s,\mathbf{r}_r)=-\frac{1}{2\pi}\int j\omega R(\mathbf{r},\mathbf{r}_s,\mathbf{r}_r)e^{-j\omega\tau(\mathbf{r},\mathbf{r}_s,\mathbf{r}_r)}\times\frac{\sin\theta_{SP}+\sin\theta_{RP}}{c}P_s(\omega)e^{j\omega\tau_i}d\omega, \tag{17}$$

which turns out to be

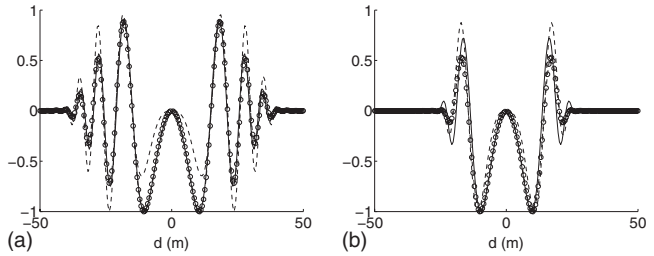

FIG. 3. [(a) and (b)] Point-to-point TSK (solid-line) versus diffraction pattern gradient (dashed) and spatially corrected diffraction pattern gradient (circle line). The three plots have been normalized according to their maxima. The source-receiver range is 1.5 km. The TSK was calculated at 750 m for a 7.6° acoustic ray for a 2.5 kHz central frequency pulse, and (a) 1250 Hz and (b) 4000 Hz frequency bandwidths.

$$\nabla_y D(\mathbf{r},\mathbf{r}_s,\mathbf{r}_r) = -\frac{1}{2\pi}\frac{\sin\theta_{SP}+\sin\theta_{RP}}{c} \times \int j\omega G(\mathbf{r},\mathbf{r}_s,\omega)G(\mathbf{r},\mathbf{r}_r,\omega)P_s(\omega)e^{j\omega\tau_i}d\omega. \tag{18}$$

Similarly, combining Eqs. (6) and (7), we can write the TSK as

$$K_i(\mathbf{r},\mathbf{r}_s,\mathbf{r}_r) = \frac{1}{2\pi}\int j\omega G(\mathbf{r},\mathbf{r}_s,\omega)G(\mathbf{r}_r,\mathbf{r},\omega)\frac{2\omega^2 P_s(\omega)}{\ddot{p}_i c^3(\mathbf{r})}e^{j\omega\tau_i}d\omega. \tag{19}$$

Equations (18) and (19) are similar but present two major differences. The first of these concerns the geometrical influence of the source/receiver position. Figure 3 shows the TSK (solid-line), the gradient of the diffraction pattern (dashed line), and the spatially corrected gradient of the diffraction pattern ($\nabla_y D(c/(\sin\theta_{SP}+\sin\theta_{RP}))$, circle line) for a 2.5 kHz central frequency signal with 1.25 and 4 kHz bandwidths, respectively. Figure 3 is obtained at a 750 m range position for a 1.5 km source-receiver range and 7.6° ray path. We can see in Fig. 3(a) that the use of the spatial correcting factor $(\sin\theta_{SP}+\sin\theta_{RP})/c$ allows a perfect fit between the TSK and the gradient of the diffraction pattern far from the waveguide interfaces. Note that this correction factor resembles the obliquity factor used in Fourier optics to account for diffraction effects from extended apertures.[27]

The second difference is more difficult to assess. The frequency contents of Eqs. (18) and (19) appear to be different, although Fig. 3(a) shows us that this is not the case. The frequency-dependent term $2\omega^2 Ps(\omega)/\ddot{p}_i c^3(\mathbf{r}')$ corresponds to the square of the acoustic wave number $(\omega/c)^2$ counterbalanced by the acceleration of the pressure-field. The acceleration of the pressure-field also justifies the missing minus term, as acceleration has an opposite phase with respect to pressure. As an illustration, Fig. 3(b) shows the same comparison performed over a larger bandwidth. We can see that the fit between Eqs. (18) and (19) is no longer perfect, since the ω^2 present in the TSK becomes significant when the bandwidth is large compared to the central frequency. We also note that the use of a wider bandwidth eliminates the side lobes of the TSK, putting sensitivity in the first Fresnel zone only. We will see below that the DBF processing leads to the same interesting phenomenon.

The similarity between Eqs. (18) and (19) is quite general and stays valid in more complicated waveguides with range-dependent and depth-dependent sound-speed patterns, as mentioned earlier. As long as we consider that the Green's function is a combination of well-identified separated eigenray contributions, we can isolate travel-time and amplitude for each eigenray connecting the source and the receiver [following Eqs. (9)–(13)], regardless of the path this ray has taken.

In conclusion, the point-to-point TSK is nothing else but the spatial derivative of the diffraction pattern that can be expected from the single-scattering (Born) approximation.

III. TSK VERSUS DIFFRACTION WITH DBF

When using DBF processes to extract eigenrays between two source-receiver arrays, the TSK reconstruction must take into account the geometry of the source and receiver arrays. More specifically, when using array processing, the measured travel-time does not correspond to the travel-time of a single arrival at one receiver $p(t)$ but corresponds to the travel-time of a linear combination of the properly time-delayed pressure-fields recorded between the source and receiver arrays. When performing the DBF analysis, the beam-formed pressure-field is given by

$$p_{\mathrm{BF}}(t,\theta_r,\theta_s) = \sum_{r=1}^{N_r}\sum_{s=1}^{N_s} a p_{rs}(t - T_r(\theta_r,z_r) - T_s(\theta_s,z_s)), \tag{20}$$

where $p_{rs}(t)$ is the pressure-field between source s and receiver r, and a_{rs} is an amplitude shading window. θ_r and θ_s are the observed receiver and launch angles, respectively, and T_r and T_s are the delay corrections to the beam-form on θ_r and θ_s. If the sound speed is uniform along the arrays, the time-delay beam-forming is

$$T(\theta,z) = (z - z_0)\frac{\sin\theta}{c}, \tag{21}$$

where $z-z_0$ is the distance between an array element at depth z and the center of the array at depth z_0.

The expression of an optimal delay correction for source-receive arrays in a depth-dependent sound-speed profile is given by the turning-point filter approach.[22] Physically speaking, the DBF consists of phasing a collection of signals according to given launch and receive angles; these are then averaged. After summation, the wave front associated with the launch and receiver angles is preserved, since it is coherently averaged, while the other field components are incoherently averaged and disappear. In this part, we investigate the spatial shape of the TSK when using DBF. As for the case of point-to-point TSK, two linearized expressions are required between δp_{BF} and δc, and between $\delta\tau_{\mathrm{BF}i}$ and δp_{BF}, to define the DBF-TSK.

As the DBF is a linear combination of pressure-fields between different source/receivers, we have the following expression:

$$\delta p_{\mathrm{BF}}(t,\theta_r,\theta_s)=\sum_{r=1}^{N_r}\sum_{s=1}^{N_s}a_{rs}\delta p_{rs}(t-T_r(\theta_r,z_r)-T_s(\theta_s,z_s)). \tag{22}$$

The linear relationship between δp and δc [see Eqs. (3) and (1)] implies a linear relationship between δp_{BF} and δc. Similarly, the relation between $\delta\tau_{\mathrm{BF}i}$ and δp_{BF} is given by Eq. (4), replacing p by p_{BF}.

Thus, using Eqs. (1), (3), (4), and (22), we define the linear relationship between the change in travel-time $\delta\tau_{\mathrm{BF}i}$ and the local perturbations of the sound-speed profile:

$$\delta\tau_{\mathrm{BF}i}=\int\int\int\delta c(\mathbf{r})K_{\mathrm{BF}i}(\mathbf{r},\mathbf{r}_s,\mathbf{r}_r)dV(\mathbf{r}), \tag{23}$$

where the TSK is now:

$$K_{\mathrm{BF}i}(\mathbf{r},\mathbf{r}_s,\mathbf{r}_r)=\frac{1}{2\pi}\int\frac{j\omega}{\ddot{p}_{\mathrm{BF}i}}Q_{\mathrm{BF}}(\mathbf{r},\mathbf{r}_{s0},\mathbf{r}_{r0},\omega)e^{j\omega\tau_i}d\omega, \tag{24}$$

with Q_{BF} as a linear combination of the point-to-point Q_{rs} expressed as

$$Q_{\mathrm{BF}}(\mathbf{r},\mathbf{r}_{s0},\mathbf{r}_{r0},\omega)=\sum_{r=1}^{N_r}\sum_{s=1}^{N_s}a_{rs}Q_{rs}(\mathbf{r},\mathbf{r}_s,\mathbf{r}_r,\omega)e^{-j\omega(T_r(\theta_r)+T_s(\theta_s))}. \tag{25}$$

When using DBF, the diffraction pattern between the two arrays is given by

$$D_{\mathrm{BF}}(\mathbf{r},\mathbf{r}_{s0},\mathbf{r}_{r0},\omega)=\sum_{r=1}^{N_r}\sum_{s=1}^{N_s}a_{rs}D(\mathbf{r},\mathbf{r}_s,\mathbf{r}_r,\omega)e^{-j\omega(T_r(\theta_r)+T_s(\theta_s))}. \tag{26}$$

If we take for D the expression in Eq. (10), and then compute the directional gradient of D_{BF} perpendicular to the ray path in the far-field approximation, we obtain the expression

$$\nabla_y D_{\mathrm{BF}}=-j\omega\sum_{r=1}^{N_r}\sum_{s=1}^{N_s}a_{rs}G(\mathbf{r},\mathbf{r}_s,\omega)G(\mathbf{r},\mathbf{r}_r,\omega)\times e^{-j\omega(T_r(\theta_r)+T_s(\theta_s))}(\nabla\tau(\mathbf{r},\mathbf{r}_s,\mathbf{r}_r)\cdot\vec{u_y}). \tag{27}$$

The spatial factor $\nabla\tau(\mathbf{r},\mathbf{r}_s,\mathbf{r}_r)\cdot\vec{u_y}$ cannot be pulled out of the sum because of its specific dependence on each source and each receiver. So we cannot deduce the TSK from the spatial derivative of the diffraction pattern by a spatial correction factor, as we did previously in the point-to-point case. However, we can approximate this correction factor by the constant $\nabla\tau(\mathbf{r},\mathbf{r}_{s_0},\mathbf{r}_{r_0})\cdot\vec{u_y}$ at the central positions r_0 and s_0 of the source-receiver arrays. Actually, $\nabla\tau(\mathbf{r},\mathbf{r}_{s_0},\mathbf{r}_{r_0})\cdot\vec{u_y}$ also corresponds to the mean value of the directional gradients. Finally, we have the approximate relationship

$$K_{\mathrm{BF}i}(\mathbf{r},\mathbf{r}_{s0},\mathbf{r}_{r0})\approx\int\frac{\nabla_y D_{\mathrm{BF}}(\mathbf{r},\mathbf{r}_{s0},\mathbf{r}_{r0},\omega)}{\sin\theta_{S_0P}+\sin\theta_{R_0P}}cP_s(\omega)e^{-j\omega\tau_i}d\omega. \tag{28}$$

Figure 4 shows a comparison between $K_{\mathrm{BF}i}$ and the righthand term in Eq. (28). As expected, the comparison degrades when the size of the source-receiver arrays is increasing.

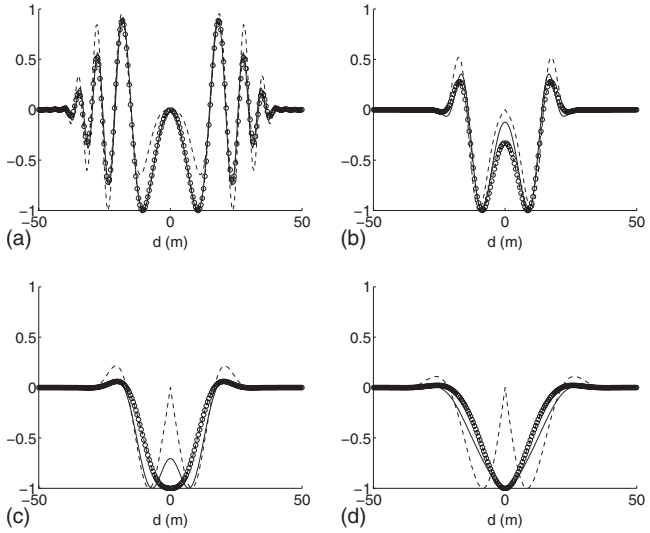

FIG. 4. (a) and (b) TSK versus the diffraction pattern gradient and spatially corrected diffraction pattern gradient, using the DBF with different array lengths. The three plots have been normalized according to their maxima. The source-receiver range is 1.5 km. TSK is calculated at 750 m for a 7.6° acoustic ray for a 2.5 kHz central frequency pulse and a 1250 Hz bandwidth. From (a) to (d), the source-receiver arrays are point to point, 30λ long, 60λ long, and 90λ long, respectively. The line codes are the same as in Fig. 3.

However, we can see that the correction factor $(\sin\theta_{SP}+\sin\theta_{RP})/c$ helps with a better approximation of the TSK from $\nabla_y D_{\mathrm{BF}}$, even in the case of the 90λ length array. In particular, we note that the directional gradient of the diffraction pattern has zero-sensitivity on the ray path, and that the spatial correction factor removes this zero-sensitivity when using arrays.

IV. ANALYSIS OF TSK USING DBF

The relationship between the TSK and the diffraction pattern of the source-receiver arrays is interesting since it can provide a simpler and faster way to calculate the TSK in shallow-water waveguides. Indeed, calculating TSK after DBF is a very time-consuming task, since it requires the computing of an ensemble of TSKs between each source-receiver pair, taken among the source-receiver arrays as required by Eqs. (24) and (25). Equation (28) shows that the TSK can be approximated from the product of the source and receiver array diffraction patterns only. For example, in the Fraunhofer approximation, the angle-dependent diffraction pattern of an N-element linear array around angle θ_0 at angular frequency ω is given by

$$B(\theta,\theta_0,\omega)=\frac{\sin(Na\omega(\sin\theta-\sin\theta_0)/2c)}{\sin(a\omega(\sin\theta-\sin\theta_0)/2c)}, \tag{29}$$

where a is the array pitch. In the far-field approximation, the diffraction pattern D_{BF} can be approximated by $B_s(\theta,\theta_s,\omega)B_r(\theta,\theta_r,\omega)$, where B_s and B_r are the diffraction patterns of the source and receiver arrays, respectively. Calculating the TSK $K_{\mathrm{BF}i}$ consists then in simply computing the directional gradient of the D_{BF} perpendicular to the ray path, weighted by the appropriate spatial correction factor, as shown in Eq. (28).

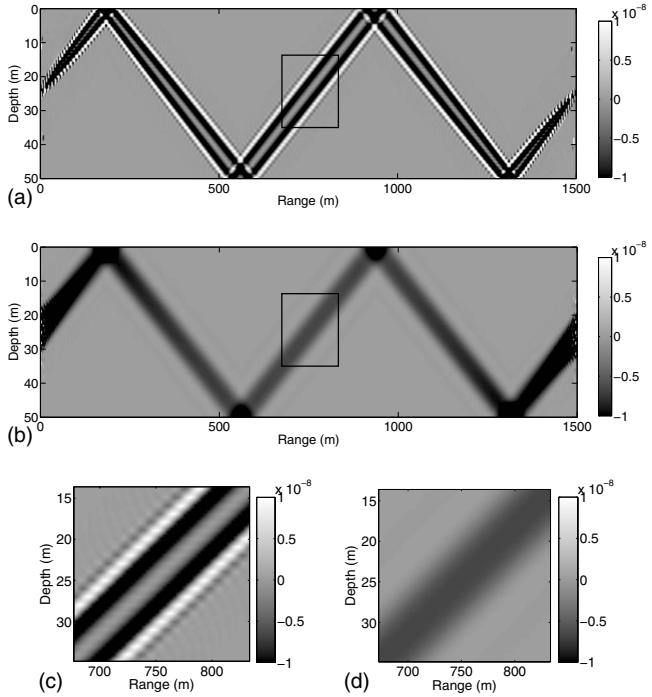

FIG. 5. TSKs ($s^2\ m^{-4}$) at 20 kHz central frequency with 30 kHz bandwidth. (a) point to point; (b) with DBF over 200−λ length arrays. [(c) and (d)] Zoom in on the central part of the ray, as defined by the black square in (a) and (b): (c) point to point; (d) with 200−λ length arrays.

Furthermore, Eq. (28) provides some physical insight in the shape evolution of the TSK with respect to the source-receiver array size. Two effects are revealed in Fig. 4. First, the side lobes become smaller when using extended antennas. This is an effect similar to the use of a larger frequency bandwidth [see the similarity between the solid-line in Fig. 3(b) and the solid-line in Fig. 4(b)]. Indeed, when integrating Eq. (29) over a frequency bandwidth Δf, it appears that an increase in Δf or array size Na leads to a similar decrease in secondary side lobes in the diffraction pattern. The same effect was seen by Raghukumar *et al.*[28] when analyzing the sensitivity kernel of a time-reversal mirror: they observed that the decrease in the sensitivity of the time-reversal focus to a sound-speed perturbation is due to the interference between more acoustic paths provided by the use of a larger array. The second effect is that the sensitivity on the ray path becomes nonzero and even becomes maximal with large aperture arrays (Fig. 4, solid-line). This result is non-intuitive, since it contradicts the well-known banana-doughnut shape classically observed with point-to-point TSK on the ray path. Indeed, as shown in Fig. 5(a), the point-to-point TSK remains zero on the ray path even at the high-frequency, large bandwidth limit. It is only the combination of TSK with DBF from source-receiver arrays that provides a non-zero-sensitivity of travel-times on the ray path. Indeed, the point-to-point zero-sensitivity on the ray path is a consequence of the stationary phase theorem that is associated to the Fermat principle that is no longer valid when the beam-forming process is performed on the source-receiver arrays.

In ocean acoustic tomography, such behavior for TSK is expected, assuming that the 3D TSK should be spatially averaged on two-dimensional (2D) sound-speed fluctuations in the ocean. In this case, TSK sensitivity on the ray path is obtained assuming a 2D TSK calculation for the sound-speed perturbation in the ocean. In our case, the maximal travel-time sensitivity on the ray path is due to the use of arrays on both sides of the waveguide and does not depend of assumptions on the shape of the ocean spatial fluctuations.

Of note, the high sensitivity seen after the DBF on the ray path is interesting from the point of view of ocean acoustic tomography. Indeed, in the limit of high-frequency, large bandwidth, and large arrays, the TSK in an acoustic waveguide shows a uniform kernel, with a sensitivity that is nearly limited to the ray path [Fig. 5(b)]. This further validates the use of ray theory and source-receiver arrays for shallow-water ocean acoustic tomography.

This last aspect of DBF and TSK leads to two interpretations. It could be said that if only a few rays are available in the waveguide, we may have more difficulties in locating anomalies, as the ambiguity of the perturbation position will now be on a broader zone. On the other hand, the uniform pattern of TSK after DBF in the Fresnel zone appears to have an advantage with respect to robustness. Indeed, sound-speed mismatch is always an issue with real data and will have a significant effect on the Fresnel zone oscillations seen on the point-to-point TSK shown in Fig. 5(c), while being negligible on the smoothly varying TSK measured after DBF [Fig. 5(d)].

V. CONCLUSIONS

In the present study, we have analyzed geometrically the mapping between TSKs and diffraction patterns. More precisely, we have shown that the point-to-point TSK is equivalent to the gradient of the diffraction pattern corrected by a spatial factor. When the pressure-field is double beam-formed on source-receiver arrays, we obtain an approximate relationship between the TSK and the diffraction pattern between the two arrays. Finally, the DBF process significantly modifies the spatial structure of TSK, in such a way that ocean acoustic tomography could improve the robustness of its performance when considering ray theory approximation.

ACKNOWLEDGMENTS

The authors would like to thank Bruce Cornuelle and Shane Walker for helpful comments on this study.

[1]P. Williamson, "A guide to the limits of resolution imposed by scattering in ray tomography," Geophysics **56**, 202–207 (1991).
[2]P. R. Williamson and M. H. Worthington, "Resolution limits in ray tomography due to wave behaviour: Numerical experiments," Geophysics **58**, 727–735 (1993).
[3]F. Dahlen, "Resolution limit of travel-time tomography," Geophys. J. Int. **157**, 315–331 (2004).
[4]J. Virieux and G. Lambaré, *Theory and Observation-Body Waves: Ray Methods and Finite Frequency Effects* (Elsevier, Amsterdam, 2007), pp. 127–155.
[5]S. Husen and E. Kissling, "Local earthquake tomography between rays and waves: Fat ray tomography," Phys. Earth Planet. Inter. **123**, 127–147 (2001).
[6]M. Woodward, "Wave-equation tomography," Geophysics **57**, 15–26 (1992).
[7]M. Born and E. Wolf, *Principles of Optics*, 6th ed. (Pergamon, New York, 1980).
[8]G. Nolet, *A Breviary of Seismic Tomography* (Cambridge University Press,

Cambridge, England, 2008).
[9]F. A. Dahlen, S. H. Hung, and G. Nolet, "Fréchet kernels for finite-difference travel-times—I. theory," Geophys. J. Int. **141**, 157–174 (2000).
[10]S. Gautier, G. Nolet, and J. Virieux, "Finite-frequency tomography in a crustal environment: Application to the western part of the Gulf of Corinth," Geophys. Prospect. **56**, 493–503 (2008).
[11]J. Tromp, C. Tape, and Q. Liu, "Seismic tomography, adjoint methods, time reversal, and banana-donut kernels," Geophys. J. Int. **160**, 195–216 (2005).
[12]M. V. de Hoop and R. D. van der Hilst, "On sensitivity kernels for 'wave-equation' transmission tomography," Geophys. J. Int. **160**, 621–633 (2005).
[13]A. Sieminski, J.-J. Lvque, and E. Debayle, "Can finite-frequency effects be accounted for in ray theory surface wave tomography?," Geophys. Res. Lett. **31**, L24614.1–L24614.4 (2004).
[14]P. Roux, W. Kuperman, W. Hodgkiss, H. C. Song, T. Akal, and M. Stevenson, "A non reciprocal implementation of time reversal in the ocean," J. Acoust. Soc. Am. **116**, 1009–1015 (2004).
[15]E. K. Skarsoulis and B. D. Cornuelle, "Travel-time sensitivity kernels in ocean acoustic tomography," J. Acoust. Soc. Am. **116**, 227–238 (2004).
[16]C. Tape, Q. Liu, and J. Tromp, "Finite frequency tomography using adjoint methods—Methodology and examples using membrane surface waves," Geophys. J. Int. **168**, 1105–1129 (2007).
[17]M. Fink, D. Cassereau, A. Derode, C. Prada, P. Roux, M. Tanter, J. Thomas, and F. Wu, "Time-reversed acoustics," Rep. Prog. Phys. **63**, 1933–1995 (2000).
[18]A. Tarantola, *Inverse Problem Theory: Methods for Data Fitting and Model Parameter Estimation* (Elsevier, Amsterdam, 1987).
[19]G. Herman, *Image Reconstruction From Projections: The Fundamentals of Computerized Tomography* (Academic, New York, 1980).
[20]A. J. Devaney, "Inverse-scattering theory within the Rytov approximation," Opt. Lett. **6**, 374–376 (1981).
[21]A. J. Devaney, "A filtered back-propagation algorithm for diffraction tomography," Ultrason. Imaging **4**, 336–350 (1982).
[22]M. Dzieciuch, P. Worcester, and W. Munk, "Turning point filters: Analysis of sound propagation on a gyre scale," J. Acoust. Soc. Am. **110**, 135–149 (2001).
[23]P. Roux, B. D. Cornuelle, W. A. Kuperman, and W. S. Hodgkiss, "The structure of raylike arrivals in a shallow-water waveguide," J. Acoust. Soc. Am. **124**, 3430–3439 (2008).
[24]M. Collins and E. Westwood, "A higher-order energy-conserving parabolic equation for range-dependent ocean depth, sound speed and density," J. Acoust. Soc. Am. **89**, 1068–1075 (1991).
[25]B. Romanowicz and R. Snieder, "A new formalism for the effect of lateral heterogeneity on normal modes and surface waves: II. General anisotropic perturbation," Geophys. J. Int. **93**, 91–99 (1998).
[26]R. Snieder and B. Romanowicz, "A new formalism for the effect of lateral heterogeneity on normal modes and surface waves: I. Isotropic perturbations, perturbations of interfaces and gravitational perturbations," Geophys. J. Int. **92**, 207–222 (1998).
[27]J. Goodman, *Introduction to Fourier Optics* (McGraw-Hill, San Francisco, 1968).
[28]K. Raghukumar, B. D. Cornuelle, W. S. Hodgkiss, and W. A. Kuperman, "Pressure sensitivity kernels applied to time-reversal acoustics," J. Acoust. Soc. Am. **122**, 3023 (2007).